Science Signaling
AAAS

www.sciencesignaling.org/cgi/content/full/3/153/rs4/DC1

Supplementary Materials for

Phosphoproteomic Analysis Reveals Interconnected System-Wide Responses to Perturbations of Kinases and Phosphatases in Yeast

Bernd Bodenmiller, Stefanie Wanka, Claudine Kraft, Jörg Urban, David Campbell, Patrick G. Pedrioli, Bertran Gerrits, Paola Picotti, Henry Lam, Olga Vitek, Mi-Youn Brusniak, Bernd Roschitzki, Chao Zhang, Kevan M. Shokat, Ralph Schlapbach, Alejandro Colman-Lerner, Garry P. Nolan, Alexey I. Nesvizhskii, Matthias Peter, Robbie Loewith, Christian von Mering, Ruedi Aebersold*

*To whom correspondence should be addressed. E-mail: aebersold@imsb.biol.ethz.ch

Published 21 December 2010, *Sci. Signal.* **3**, rs4 (2010)
DOI: 10.1126/scisignal.2001182

This PDF file includes:

Other Supplementary Material for this manuscript includes the following:
(available at www.sciencesignaling.org/cgi/content/full/3/153/rs4/DC1)

Table S1 (Microsoft Excel format). List of enzymes.
Table S3 (Microsoft Excel format). Information on phosphopeptides and phosphoproteins.
Table S6 (Microsoft Excel format). Confirmed STRING interactions.
Table S11 (Microsoft Excel format). GO terms.
Table S13 (Microsoft Excel format). Information on yeast strains.

Materials and Methods

General comments

All chemicals and reagents, unless noted otherwise, were purchased at the highest available purity from Sigma-Aldrich, Taufkirchen, Germany.

Generation of haploid yeast kinase deletion strains

The bait strains BY7092 and BY7220 were kindly provided by Charlie Boone, Toronto. Heterozygous diploid yeast strains harboring the kinase deletions were obtained from Euroscarf (http://www.uni-frankfurt.de/fb15/mikro/euroscarf/index.html) and grown in a 384-array format. After sporulation, the resulting spores of these strains were mated against a haploid bait strain BY7092 (Mat alpha, *can1::STE2pr-Sp_his5 lyp1Δ his3Δ leu2Δ ura3Δ met15Δ*) containing the plasmid pRS316 (strains labeled "derived from BY7092", table S13), or against the strain BY7220 (Mat alpha, *can1::STE2pr-Sp_his5 lyp1Δ cyh2Δ his3Δ leu2Δ ura3::NatR met15Δ*) (strains labeled "derived from BY7220", table S13). Haploid cells were selected according to the procedure described by Tong and Boone (*1*) with the following modifications for strains derived from BY7092: Diploid selection was performed on MSG-U +G418 for 3 days at 30ºC followed by growing on YPD + G418 for 1 day at 30ºC. Sporulation was performed in the absence of Ura, and the final meiotic progeny selection was performed in the absence of clonNat. Strains derived from BY4743 (table S13) were obtained after dissecting sporulated heterozygous diploid deletions strains. The genotype of these strains is as follows: S288C (Mat a, *his3Δ1 leu2Δ0 met15Δ0 ura3Δ0*), unless otherwise noted. The correct location of the kanamycin-resistance cassette was verified by PCR in all strains with Phusion Polymerase (Finnzymes), which was used according to the manufacturer's specifications, and primers as found under the *Saccharomyces* Genome Deletion Project Web page (http://www-sequence.stanford.edu/group/yeast_deletion_project/deletions3.html), which are detailed in the "Primer Sequences" section: (http://www-sequence.stanford.edu/group/yeast_deletion_project/Deletion_primers_PCR_sizes.txt).

Generation of analog-sensitive kinase strains

Genes were amplified by PCR and cloned into the vector pRS416. Gate-keeper residues in the ATP-binding pocket of a given kinase were mutated to glycine or alanine (the position of the amino acids is indicated below) by fusion PCR and constructs were verified by sequencing. Diploid strains carrying a deletion of the respective gene were transformed with the appropriate plasmid and were then sporulated. The resulting haploid strains were tested for sensitivity to 5-FOA and to various ATP analogs (*2*).

The genotypes of the strains used for phosphoproteomics are as follows:

bur1::KanMX, LYS2, met15 + pJU 1164 *(BUR1)*
bur1::KanMX, LYS2, met15 + pJU 1179 *(BUR1 - L149G)*

cdc15::KanMX, lys2, MET15 + pJU 1167 *(CDC15)*
cdc15::KanMX, lys2, MET15 + pJU 1175 *(CDC15 - L99G)*

cdc28::KanMX, LYS2, met15 + pJU 1189 *(CDC28)*
cdc28::KanMX, LYS2, met15 + pJU 1203 *(CDC28 - F88G)*

hrr25::KanMX, LYS2, met15 + pJU 1163 *(HRR25)*
hrr25::KanMX, LYS2, met15 + pJU 1197 *(HRR25 - I82G)*

mps1::KanMX, LYS2, met15 + pJU 1166 *(MPS1)*

mps1::KanMX, LYS2, met15 + pJU 1181 *(MPS1 - M516G)*

rio1::KanMX, LYS2, met15 + pJU 1168 *(RIO1)*
rio1::KanMX, LYS2, met15 + pJU 1173 *(RIO1 - M195G)*

cbk1::KanMX, LYS2, MET15 + pJU 1194 *(CBK1 - M429A)*

kin28::KanMX, LYS2, met15 + pJU 1161 *(KIN28)*
kin28::KanMX, LYS2, MET15 + pJU 1172 *(KIN28 - L83A)*

Determination of inhibitor sensitivity
To determine both the optimum inhibitor and the concentration at which it should be added to the yeast culture, we used spot assays. The following combinations (see plates below) were found to inhibit growth of the mutant strains at a final inhibitor concentration of 3 μM.

Kinase	***Inhibitor (see below for detailed description)***
Bur1	3-MB-PP1 (*3*)
Cdc15	Bn-PP1 (*4*)
Cdc28	3-MB-PP1 (*3*)
Hrr25	3-MB-PP1 (*3*)
Mps1	3-MB-PP1 (*3*)
Rio1	Bn-PP1 (*4*)
Cbk1	2-MB-PP1 (*5*)
Kin28	1-NA-PP1 (*6*)

Growth of yeast strains: deletion mutants
The yeast strains were streaked out on an appropriate plate and three biological replicates (from three single colonies) for each of the *S. cerevisiae* wild-type and deletion strains were grown to an OD of ~0.8 at 30°C in synthetic defined (SD) medium [per liter: 1.7 g yeast nitrogen base without amino acids (Chemie Brunschwig), 5 g ammonium sulfate, 2% glucose (w/v), 0.03 g isoleucine, 0.15 g valine, 0.04 g adenine, 0.02 g arginine, 0.02 g histidine, 0.1 g leucine, 0.03 g lysine, 0.02 g methionine, 0.05 g phenylalanine, 0.2 g threonine, 0.04 g tryptophan, 0.03 g tyrosine, 0.02 g uracil, 0.1 g glutamic acid and 0.1 g aspartic acid). Because we wanted to make sure that the yeast cultures at the chosen harvesting conditions were still in the log phase as well as having an excess of glucose, we determined the growth curve of the wild-type strain in the medium used and determined the glucose concentration at distinct time points. We found that when grown to an OD of ~0.8, there was still an excess of glucose in the medium.

Growth of yeast strains: inhibitor sensitive mutants
Growth and harvesting were performed as described for the deletion mutants with the following differences. Because of the limited availability of the inhibitors, only single cultures were grown of each strain carrying the plasmid with the kinase gene or the strain carrying the plasmid with the inhibitor sensitive kinase gene [of each resulting phosphopeptide isolate, three technical replicates were measured by LC-MS(/MS)]. Then, inhibitor was added at a final concentration of 3 μM to the liquid cultures for 23 min.

Harvesting of yeast cells
Trichloroacetic acid (at a final concentration 6%) was added directly to the yeast cultures, which were then placed for 10 min into ice water. The yeast cells were pelleted by centrifugation at 1,500*g*, the supernatant was discarded, and the cells were resuspended in ice-cold acetone. After another round of centrifugation at 1,500*g*, the pellet was washed once more with ice-cold acetone, the supernatant was removed, and the pellet was frozen at -80°C until required for further processing.

Processing of the yeast pellets
The yeast cells were subsequently lyzed by beating with glass beads in 8 M urea, 50 mM ammonium bicarbonate, and 5 mM EDTA. Debris was removed by centrifugation at 16,000*g*. Protein concentration was determined with a BCA protein assay kit (Pierce). Then, for each replicate, 3.5 mg of total protein were reduced, alkylated, digested, and prepared for phosphopeptide isolation as described previously (*7*). For 16 mutants and the wild-type strain, several microgram of the peptide mixture were saved to quantify changes in protein abundance.

Phosphopeptide isolation
The phosphopeptides were isolated with titanium dioxide (TiO_2, GL Science) from the proteome digest as previously described (*7*) with slight modifications. 3.5 mg of peptides were reconstituted in 280 µl of a solution containing 80% acetonitrile (ACN) and 3.5% trifluoroacetic acid (TFA), which was saturated with phthalic acid. The peptide solution was added to 1.2 mg of equilibrated TiO_2 in a blocked Mobicol spin column (MoBiTec) and was incubated for 30 min with end-over-end rotation. The resin was thoroughly washed twice with 280 µl of the above described saturated phthalic acid solution, twice with 280 µl of a solution of 80% ACN and 0.1% TFA, and twice with 280 µl of 0.1% TFA. Phosphopeptides were eluted twice with 150 µl of 0.3 M NH_4OH. After elution, the pH was rapidly adjusted to 2.7 with 10% TFA, and phosphopeptides were purified with an appropriate C18 cartridge.

Mass spectrometric analyses of yeast phosphopeptide isolates
All phosphopeptide (and peptide) samples were analyzed on a hybrid LTQ-Orbitrap mass spectrometer (ThermoFischer Scientific) interfaced with a nano-electrospray ion source. Chromatographic separation of peptides was performed on an Eksigent nano-LC system (Eksigent Technologies), equipped with an 11-cm, fused silica emitter, which had an inner diameter of 75 µm inner diameter (BGB Analytik), packed in-house with a Magic C18 AQ, 5- or 3-µµm beads, loaded from a cooled (4°C) Spark Holland autosampler, and were separated with an ACN/water solvent system containing 0.1% formic acid, with a flow rate of 200 nl/min. Phosphopeptide mixtures were separated with a gradient from 4 to 24% ACN over 60 min. For MS/MS data acquisition, one to three data-dependent MS/MS scans were acquired in the linear ion trap for each Orbitrap-MS scan, the latter acquired at 60,000 full width at half maximum (FWHM) nominal resolution settings, with an overall cycle time of ~1.2 s. To maximize the number of peptide identifications, a different charge state screening was employed for each of the biological replicates (no technical replicates were measured, except for the analog-sensitive strains). Either only 2+ ions were selected, rejecting 1+, 3+, and higher charged ions and those with undetermined charge or only 3+ and higher charged peptides were selected, excluding 1+, 2+, and undetermined charges. In addition, for some runs, multistage activation was employed with 98 D, 49 D, 32.66 D, and 24.5 D defined as the neutral loss masses. For injection control, the automatic gain control (AGC) was set to 5×10^5 and 1×10^4 for full Orbitrap-MS and linear ion trap MS/MS, respectively. The instrument was

calibrated externally, according to the manufacturer's instructions. Data were acquired with an internal lock mass calibration at m/z 429.088735 and 445.120025.

Database searches

The MS2 data were searched against a decoy/non-decoy version of the *Saccharomyces* Genome Database SGD non-redundant database containing 13,590 protein entries (6,795 forward protein entries and 6,795 reversed protein entries) with SORCERER-SEQUEST v3.0.3 software which was run on the SageN Sorcerer2 (Thermo Electron). For the in silico digest, trypsin was defined as the protease, cleaving after lysine (K) and arginine (R); if followed by proline (P), the cleavage was not allowed. Two missed cleavages and one non-tryptic terminus were allowed for the peptides which had a maximum mass of 6,000 D. The precursor ion tolerance was set to 7 ppm and fragment ion tolerance was set to 0.5 D. The data were searched under the conditions that phosphorylation (+79.9663 D) of serine, threonine, and tyrosine was defined as a variable modification and carboxyamidomethylation of cysteine (+57.0214 D) was defined as a fixed modification. For the non-phosphopeptide samples, no variable modification was defined. Finally, the search results obtained by Sequest were subjected to statistical filtering by PeptideProphet (V3.0) (*8*). A PeptideProphet cut-off of 0.9 was chosen, which had to be met before a peptide was considered as correctly identified. Because not all of the identified tandem mass spectra could be mapped back to their corresponding MS1 peptide ions, we furthermore determined the false discovery rate (FDR) of the annotated peptide ions, separately for each phosphorylation pattern. For that purpose, we kept the PeptideProphet probability cut-off of 0.9, and used the target-decoy entries present to determine the FDR (*9*). The resulting false positive rates are shown in table S7, and were on average 3.8%. In addition, only phosphopeptide isolates that showed a strong enrichment in phosphopeptides were considered for further processing (table S7). The specificity of the phosphopeptide enrichment was computed for each given comparison between wild-type and mutant phosphorylation patterns and all (phospho)peptides with a PeptideProphet score >0.9 as (#phosphopeptides)/((#all peptides)*100). Note that because in our computational pipeline the identification of phosphopeptides was penalized compared to that of non-phosphopeptides, it is correct to assume that the specificity of isolation was even greater than the determined average of 80%.

Localization of phosphorylation sites

Beausoleil *et al.* described an algorithm that computes the probability of whether the localization of a phosphorylated amino acid residue within a peptide is correct, which is called the AScore (http://ascore.med.harvard.edu/) (*10*). For this work, we adopted a custom version of this algorithm to be executable on PeptideProphet (V3.0) (*8*) output files after the Sequest database search. A detailed description of our AScore version was previously described (*11*). The maximum and average AScore values for the phosphopeptides of this study are shown in table S3.

Data availability

All data, including the mass spectra, can be viewed in the PhosphoPep (http://www.phosphopep.org) database (*12, 13*).

Quantification of phosphopeptide ions

For the detection of the regulated features (ion peak detection, computation of the peptide ion area from the LC-MS data, alignment of the features over multiple LC-MS runs, and annotation of each features with the phosphopeptide sequence), we used the SuperHirn algorithm (v2.0), as described by Mueller *et al*. (*14*). The most important parameters used in SuperHirn were as follows:

```
//        GENERAL:
//
//        retention time tolerance:       tolerance with which lc-peaks will be merged
//                                        AFTER the alignment of the spectra [min]
MS1 retention time tolerance=2.5
//
//        mass time tolerance:            mass tolerance with which lc-peaks will be merged
//                                        AFTER the alignment of the spectra [Da]
MS1 m/z tolerance=0.01
//
//        MS2 m/z tolerance:              mass tolerance with which MS2 identifications will be
associated
//                                        to a defined MS1 LC elution peak [Da]
MS2 m/z tolerance=0.008
//
//        MS2 mass matching modus:              define which modus used to match ms2
assignments to ms1 peaks
//                - theoretical mass [1]  : use theoretical mass calculated from sequence
//                - MS1 precursor mass [0]: use measured ms1 mass of precursor ion
MS2 mass matching modus=1
//
//
// Peptide Prophet Threshold:  threshold used in clustering peptides into proteins
//
Peptide Prophet Threshold=0.5
//
//        MS2 SCAN tolerance:                   SCAN tolerance with which MS2 identifications
will be associated
//                                        to a defined MS1 LC elution peak []
MS2 SCAN tolerance=150
//
//        MS2 retention time tolerance:         retention time tolerance with which MS2
identifications will be associated
//                                        to a defined MS1 LC elution peak [min]
//                                        (if set to -1, then the MS1 retention time tolerance will be
used
MS2 retention time tolerance=5
//
//        IL MS2 SCAN tolerance:                SCAN tolerance with which MS2 info FROM
INCLUSION LIST will be associated
//                                        to a defined MS1 LC elution peak []
INCLUSIONS LIST MS2 SCAN tolerance=200
//
//
```

```
//        PPM MS2 MZ modus:     defines if PPM values should be used in the assigment of MS2 info to MS1 features
//                  if set to 1, then matched via PPM value, otherwise via mz tolerance
//                    (adjust then also the parameter<MS2 PPM m/z tolerance> according to your experiment!) 1=on, 0=off
//
PPM MS2 matching modus=1
//
//        MS2 PPM m/z tolerance:              mass tolerance with which MS2 identifications will be associated
//                  to MS1 features. same as parameter <MS2 m/z tolerance> but in PPM
//                  to activate, set parameter <PPM MS2 matching modus> to 1!
MS2 PPM m/z tolerance=5
//-----------------------------------------------------------------------------------------------------
//
//        MS1 feature selection options
// these options apply to the selection of MS1 feature from the XML/APML format
// they do not apply to the basic extraction of features from the raw mzXML data
//
//        elution window:                     enables to only process a period of the
//                                  elution gradient, defines by start / end
//                                  only peaks within this region are accepted!!!, [min]
start elution window=15.0
end elution window=110.0
//
//        LC peak score cutoff:         above which are LC peaks accepted,otherwise discarted
LC peak score cutoff=10000
//
//        LC peak intensity cutoff:     only MS1 feature at or over this intensity level are accepted, otherwise discarted
MS1 feature intensity cutoff=10000
//
// Charge state min:  For the selection of MS1 features by charge state, here its, the minimal charge state:
MS1 feature CHRG range min=2
//
// Charge state max:  For the selection of MS1 features by charge state, here its, the maximal charge state:
MS1 feature CHRG range max=5
//
// M/z min:  For the selection of MS1 features by m/z, here its, the minimal m/z value:
MS1 feature mz range min=300
//
// M/z max:  For the selection of MS1 features by m/z, here its, the maximal m/z value:
MS1 feature mz range max=1600

//
//        STORAGE OF DATA IN THE XML MASTER AND LC-MS FILE:
// ( 0 = no, 1 = yes )
//
```

```
//        store only best MS2 per feature      :      only the best MS2 scan / feature will be store in the XML file
//                                                    (LC-MS runs and MasterMap) use to reduce XML file size
store only best MS2 per feature=0
//
//        store only best MS2 per ALIGNED feature :      only the best MS2 scan / ALIGNED feature will be store in the XML file
//                                                    (LC-MS runs and MasterMap) use to reduce XML file size
store only best MS2 per ALIGNED feature=0
//
//        nb. max. alternative protein names : max. number of alternative proteins that will be store in the XML file
//                                                    for a non proteotypic peptide
nb. max. alternative protein names=5
//-------------------------------------------------------------------------------------------------
//
//        ALIGNMENT OF LC_MS SPECTRA:
//
//        Window retention time:          retention time window (min) to search
//                                    for common peaks BEFORE the alignment.[min]
retention time window=5.5
//
//        mass window :               mass window (DA) to search for common
//                                    peaks BEFORE the alignment. [Da]
mass / charge window=0.008
//
// smoothing error TR window:         used to copmute the alignment error, use a tr window to
//                                    calculate the standard deviations of raw data to predicted
//                                    delta shift [min]
smoothing error TR window=1.0
//
//        max. nb. stripes:           in the plot of TR A vs TR B, there are off diagnal
//                                    horizontal and vertical stripes, which come from
//                                    high abundance long eluting peptides.
//                                    allow only such stripes of max. length around the diagonal [#]
max. nb. stripes=1
//
//        sequence alignment comparsion:      defines the weight with which peptide identification information
//    is used in the matching of common lc/ms peaks between runs ( 0(not used) - 5000)
MS2 info alignment weight=0
//
//        maximal smoothing error:    when calculating the upper / lower error of the fitted delta
//                                    do not allow an error that is bigger then this paramater [min]
maximal smoothing error=3.0
```

```
//
//        % outside error delta points: how many percentage of points can still lay outside the alignment error
//                                      borders in order to stop the alignment iterations
//
perc. outside error delta points=0.75
//-------------------------------------------------------------------------------------------------------
//
// LC-MS  correlations
//
//        intensity bin size:           used to correlate 2 LC-MS peaks also by their intensity
//                                      compares in which bin the 2 peaks are, for this use a bin size
intensity bin size=2000
//
//        intensity bin tolerance:      in the comparison of intensity bins, how far to bins can be appart
//                                      and still be accepted for same
intensity bin tolerance=2
//
//        min. LC/MS correlation score:       represents the worst score possible, this one will be used to
//                                      normaize the observed scores between 0(bad) and 1(good) [ 0 ... 1]
minimal LC/MS score=0.1
//
//        LC/MS sim. score modus:       which scoring system to use for LC/MS similarity:
//     - [ALIGN]: asssessment of uncertainty in the alignment
//     - [INTNES]: asssessment of ranking correlation of peak areas
//     _ [PEAK_MATCHING]: according to how many features overlap
//     _ [TOTAL]: combination of all scores:
//     _ [NORM_TOTAL]: normallized score of total score:
LC/MS sim. score modus=TOTAL
//-------------------------------------------------------------------------------------------------------
//
// MS1 PEAK DETECTION PARAMETERS FOR THE DIFFERENT FILTER METHODS:
//
//  Create monoisotopic LC profile:  to create and store the original profile of the detected
//                                   monosiotopic pecursors in the XML (!!! increases the
//                                   XML file size!!! (on[1]/off[0])
Create monoisotopic LC profile=1
//
//
//        FT MS1 data centroid data   :       define if ipnut FT-LTQ data is in centriod mode (1)
//                                   or ectract data from profile mzXMLs (0)
FT MS1 data centroid data=0
//
//        mz cluster tolerance   :      defines which tolerance is used to cluster different
//                                   m/z values into a m/z cluster
FT peak detect MS1 m/z tolerance=0.01
```

```
//
//
//        MS1 minimal # peak members:       minimal number of members in an LC elution peak, if
//                                          an elution peaks is discarded if it has less member
FT peak detect MS1 min nb peak members=4
//
//        MS1 minimal intensity     :       all peaks with small intensity are not considered
FT peak detect MS1 intensity min threshold=20000
//
//        MS1 intensity cut off :           used to discard peak with too low intensity in a
//                                          LC elution cluster. peak which are less x% of the
//                                          cluster apex peak intensity are removed [ 1 .. 0]
MS1 intensity apex percentil cutoff=0.1
//
//        MS1 max scan member distance:     defines how many scans can be between members of
//                                          a LC elution peak (MS2 scans are not inlcuded!!!)
MS1 max inter scan distance=5
//
//        Tr resolution:  used for to compute the peak area of an LC peak
//                                          in the integration process
MS1 LC retention time resolution=0.01
//
//        Peak detection absolute mass precision in Dalton (between isotopes) 0.01
Absolute isotope mass precision=0.05
//
//        Peak detection relative mass precision in ppm (between isotopes) 10
Relative isotope mass precision=10
//
//        Centroid is calculated in window of this size around local maxima
Centroid window width=5
//
//        Coefficient of variance for intensities (also includes deviation from
IntensityCV=0.9
//
//        Factor (f) to define which isotopic peaks are detectable relative to highest isotopic peak I_max: I_iso > I_max*f
Detectable isotope factor=0.2
//
//        Minimal peak height (peaks smaller than this values are not considered as monoisotopic peaks)
Minimal peak height=0.0
//
//        Intensity values below this value are considered as zero (before peak detection)
Intensity ground level=1.0
//
//        Report all found monoisotopic peak to file mono_peaks.txt
Report mono peaks=0
//
// Directory where debug files are written
```

Debug directory=
//
// if "Report mono peaks"==1 the info about the peak detection at this scan number will be written to debug files
Report scan number=0
//---
//
// STATISTICS TOOLBOX:
//
// NORMALIZATION OF INTENSITY ACROSS LC_MS RUNS IN MASTER RUN:
//
// intensity coeff. window : windows size to slide over LC elution time scale and
// compute an intensity normalization coefficient [min.]
intensity coeff. window=3
//
// Retention time step: value of the retention time step to calculate the
// intensity normalization coefficient [min.]
retention time step=1.0
//
// feature align percentage: normalization between n LC-MS runs is performed on features aligned
// across all n runs. to allows flexibility, this parameters allows to specify
// across what percentage of runs the feature has to be aligned [0 ... 1.0]
normalization feature align percentage=1.0

Post-processing of SuperHirn results to avoid signals caused by missed feature alignment

Occasionally, SuperHirn fails to correctly align some of the phosphopeptide features from multiple LC-MS/MS runs. If such an alignment failure occurs when comparing mutant and wild-type samples, then it can lead to erroneous inference of a "reliable" change in phosphopeptide abundance in response to a mutation (for example, in cases where the peptide feature happens to be aligned in all three wild-type samples, but not in the mutant samples). To avoid such false signals, we identified potential mis-aligned features in a post-processing step and, in each case, merged them to a single representative feature. Essentially, we identified mis-aligned features based on similarities in mass and retention time (allowing for a certain "window" of tolerance). In a first step, we only considered features that had MS2 information and a PeptideProphet score of >0.9. We created clusters of potentially mis-aligned features by grouping those with the same peptide sequence, mass, and retention time. For both mass and retention time, we permitted tolerances of 15 ppm for mass and 7 min for retention time; the latter tolerance was increased to 15 min at the beginning and end of each LC separation run. MS2 sequences had to be identical, except with respect to the exact position of the phosphorylated residue (allowing a shift of a maximum of 5 residues). In a second step, we extended the clusters by including non-MS2-features. For these, more stringent tolerance intervals were used: 3 ppm mass tolerance, and a 3- or 5-min retention time tolerance. Finally, the features of every cluster were merged to a single representative feature. The intensity values were added run-wise, the average mass of all features was used as the new aligned feature mass, and for retention time and charge, the full range was provided. The MS2 data of an aligned feature were represented by a non-redundant list of all of the encountered sequences. For features that were apparently partitioned exactly along the wild-type–mutant distinction (that is, observed in the wild-type, but never observed in the mutant), we intentionally increased the window of tolerance to make sure that these observations were real (that is, we erred to be on the safe side here, even if this occasionally meant the loss of a real signal). For these features, tolerances were 25 ppm mass tolerance and 15 or 20 min retention time in the first step, and 3 ppm mass tolerance and a 5- or 7-min retention time in the second step. All tolerance-values stated above were chosen based on manual inspection of the data, with the simple rule that distinct features with matching MS2 identification should be merged, but that features with incompatible MS2 identifications should not be merged. In the entire post-processing pipeline, only features with a signal-to-noise-ratio better than 10 were considered (for features that seemed to appear or disappear in the comparison between wild-type and mutant, the signal-to-noise-ratio threshold was increased to 60), assuming as background noise level in a given run the average of the 50 lowest signals as detected by SuperHirn. With respect to the MS2 sequences, half-tryptic peptides were discarded and all other peptides were merged with the corresponding peptide. Finally, we performed two manual validation steps before continuing with the data analyses. First, for very few cases, peptides indicating the gene product of a knock-out were observed. If an explanation for this observation could be found (low peptide probability or wrong peptide identification, sample carry over, mis-assignment, etc.) the entries were removed. If not, the master maps were omitted from further analyses. Second, we plotted the extracted ion chromatograms for all phosphopeptide ions that were only detected either in the wild-type or mutant replicates to manually validate their presence or absence ("vanished"/ "appeared").

Statistical significance of observed differential abundances of phosphopeptides

After post-processing of the SuperHirn output files, the phosphopeptides were separated into different statistical classes for further analysis. A class consisted either of phosphopeptides for which the MS1 signal was detected in all replicates (three times for the wild-type and three times for the mutant) or of phosphopeptides for which 1, 2, 3, or up to 5 signals were missing.

The category "3 signals missing" was further separated into phosphopeptides for which either (i) the signal was reproducibly present in either all wild-type or all mutant samples, or (ii) the signal was spread over all wild-type and mutant samples. Before statistical analysis, the missing data values were imputed with the integrated background noise as determined by the SuperHirn algorithm. These datasets were then further analyzed as described in detail previously (*15, 16*). In short, the employed software tool called Corra (*17*) wraps around the Limma (*16*) software package, which is available from the R-based project Bioconductor, and performs a statistical test comparing the abundances of a feature between the mutant and the wild type replicate samples. The test is an Empirical Bayes alternative to the Welsh *t* test, and is based on a moderated *t* statistic where the standard error is calculated with the information from all of the analyzed phosphopeptide features. Overall, the statistical analysis that we used assumes that the abundances of each feature follow a normal distribution across runs. (Normality analysis of our dataset showed that deviations to normality, even if present, were minor; the same was true for the assumption of equal distribution of our features.) Even if this assumption was not always fulfilled, the test statistics and their associated *P* values remain useful to detect changes in abundance. The test is conducted separately for each feature and each mutant.

When the number of replicate samples in the experiment is small, inference based on the *t* test may be somewhat unstable. The Empirical Bayes (or moderated) alternative to the *t* test, originally developed for gene expression microarrays (*16, 18*), is designed to remedy this problem. It combines the information regarding feature variability across all features, and improves both the sensitivity and specificity of finding the true changes in abundance across sample types. The resulting *P* value is then adjusted for multiple comparisons according to the procedure by Benjamini and Hochberg, which controls the FDR (*19*). A potential technical problem with the application of the procedure is the positive correlation in abundances of multiple peptides from the same differentially abundant protein, as well as an increased positive correlation between test statistics due to the use of the Empirical Bayes procedure. However, Benjamini *et al*. (*20*) demonstrated that calculations of the FDR are robust to positive inter-feature correlation. Therefore, the application of the procedure to our dataset was appropriate. As has been described for microarray data (*21*), a major factor for the reproducibility of a given regulation is the observed fold-change. Therefore, besides using the FDR cut-off of 0.015, we also required the fold-change in the abundance of a phosphopeptide to be equal or greater than a $\log_2$ of 1.5 to consider it as regulated. For features that were only seen in either the wild-type or the mutant ("vanishers" or "appearers"), this cut-off was raised to $\log_2 > 4$ to exclude the possibility that phosphopeptide ions just above (or below) the MS detection limit were detected to vanish (appear).

Changes in the extent of phosphorylation versus changes in protein abundance

For the first analysis (comparison of the changes in the abundance of phosphopeptides with those of non-phosphorylated peptides) the following deletion mutants were analyzed:

YCR079W

YGL059W

YGR040W

YHR135C

YKL171W

YOR231W

YBL088C

YDL079C
YDL101C
YGL180W
YGR092W
YJL128C
YLR248W
YNL307C
YPL140C
YPL141C

For the second analysis, all regulatory events were considered independently, provided that (i) at least one phosphopeptide was significantly regulated, and (ii) a second phosphopeptide mapped to the same phosphoprotein, irrespective of whether or not it was also observed as significantly regulated. Note that responses with opposite directionality are actually not expected to occur very frequently: They require both the disappearance and the appearance of specific phosphopeptides in response to deletion of the same kinase or phosphatase.

Global impact of kinases and phosphatases on the phosphoproteome
When computing the impact of a given kinase or phosphatase, we first normalized the number of regulated phosphopeptides to all of the identified phosphopeptides of that given kinase or phosphatase and to the total number of regulated phosphopeptides (see Fig. 2). The enzymes were then ranked according to their normalized impact. Note that the determined numbers were just an estimate, because of (i) experimental variations between analyzed batches and therefore differences in LC-MS maps; (ii) the incomplete covered phosphoproteome; and (iii) our computational approach of performing pair-wise comparisons between wild-type and mutant samples. We considered kinases or phosphatases as shown in Fig. 3A to be active if 10 or more phosphopeptides changed significantly in abundance upon deletion of the kinase or phosphatase or upon inhibition of the essential kinase.

Computation of the biological processes enriched in the inactive and active kinases and phosphatases
For this analysis, we only considered the gene deletion strains, because the inhibitable strains are not representative as a result of the variability in the impact on the phosphoproteome depending on the length of time of inhibition, for example. The enrichment analyses were performed with http://pipe.systemsbiology.net using the default settings (yeast proteome background).

Because the following terms are associated with the kinases and phosphatases themselves, we removed them from the results shown:

phosphate metabolic process
phosphorus metabolic process
protein amino acid phosphorylation
phosphorylation
post-translational protein modification
protein modification process
biopolymer modification
cellular protein metabolic process

protein metabolic process
cellular macromolecule metabolic process
signal transduction
cell communication
biological regulation
dephosphorylation
biopolymer metabolic process
protein amino acid dephosphorylation
regulation of biological process
regulation of cellular process
macromolecule metabolic process
regulation of biological process
regulation of cellular process
response to stimulus

Computation of the biological processes enriched among all responding proteins for a given kinase or phosphatase

For each kinase or phosphatase, the regulated phosphopeptides were mapped to their corresponding proteins. In case phosphopeptides mapped to several proteins, only those peptides mapping to homologous proteins (with equal biological processes) were retained. The enrichment of GO biological process terms was calculated with the hypergeometric test–based *GOstats* package version 2.8.0 and the yeast annotation package *org.Sc.sgd.db* version 2.2.6 from Bioconductor. Only GO terms with a *P* value <0.01 were considered. All values in table S11 are given in $\log_2$.

Determination of morphological phenotypes

The morphological phenotypes of all strains (table S4) were determined as described by Gordon *et al*. (*22*). Furthermore, phenotype data as measured by Ohya *et al*.(*23*) and growth speed as determined by Hillenmeyer *et al*. (*24*) were used for the analyses. A strain was considered to have a strong growth phenotype ("+") or very strong growth phenotype ("++") if it grew between to between 30 to 100%, >100% as fast/slow as the wild-type strain under the same growth conditions. A strain was considered to have a strong morphological phenotype ("+") or a very strong morphological phenotype ("++") if at least one or more than 10, respectively, of the 254 parameters had a significance equal to or smaller than 1×10^{-05}.

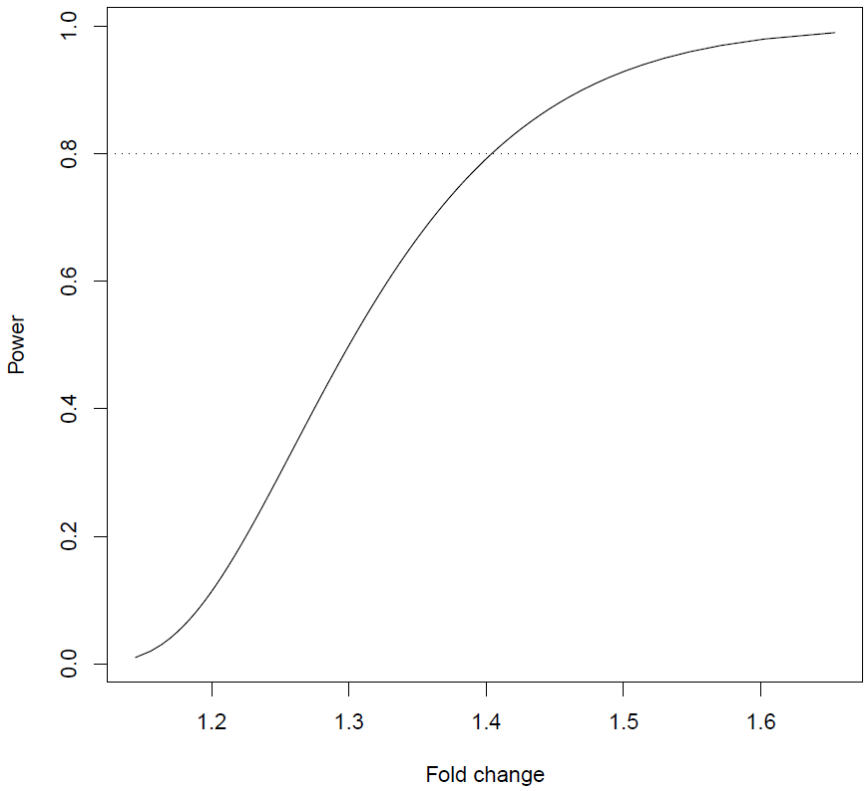

Fig. S1: Power of the analysis approach. The results of the Empirical Bayes approach were used to provide estimates of the power of our analysis, as described (*25*). Specifically, we took the median of posterior estimates of feature-specific variances provided by the Empirical Bayes *t* test, and the proportion of statistically significant changes in the datasets as input parameters. We set the FDR threshold to 0.1 and varied the expected fold-change between 1.0 and 1.7. The figure displays the power of the statistical test in this setting.

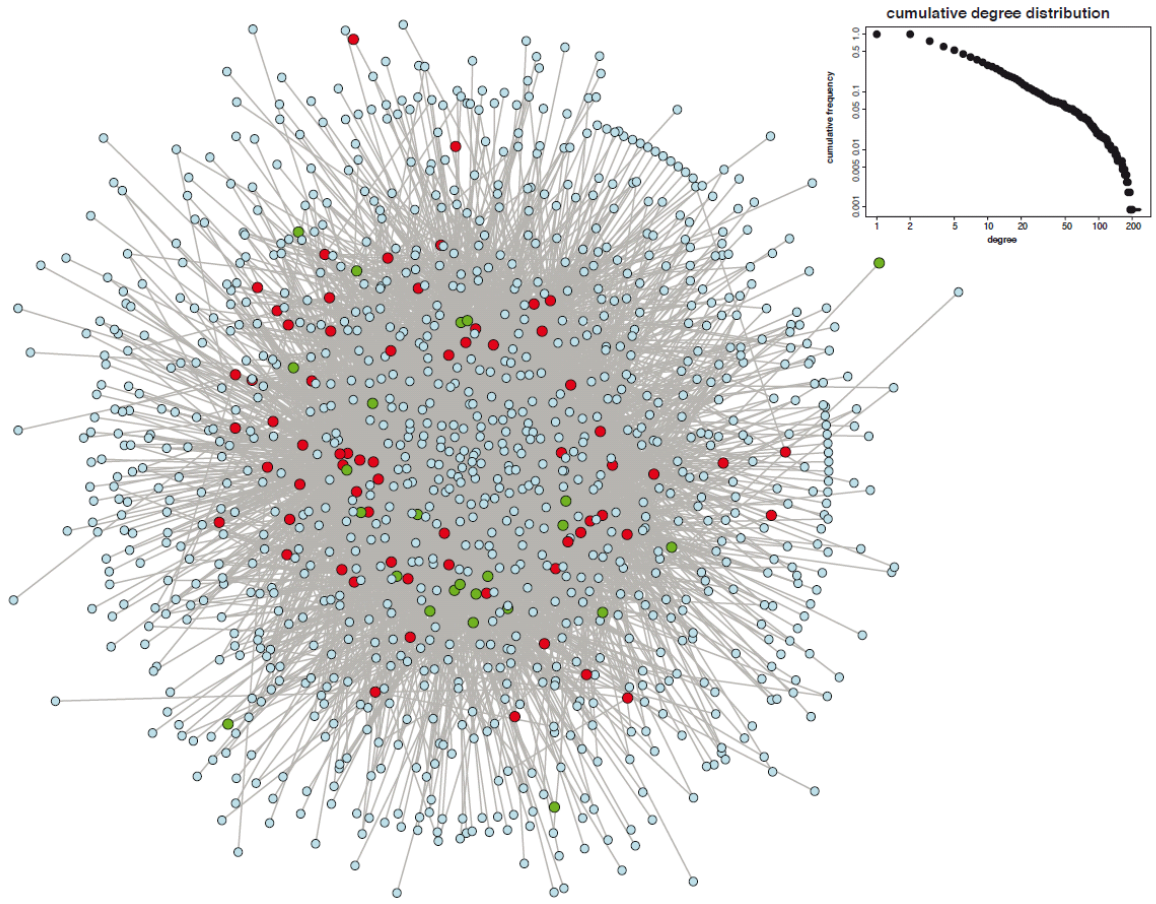

Fig. S2. Topological properties of the protein phosphorylation network. The network shown, which contains 1,088 nodes and 6,509 unique edges, is a summary view of the connectivity observed in our dataset. Kinases are shown in red, phosphatases in green, and responder proteins in light blue. Lines indicate substantial regulatory events. Inset: degree distribution of network connectivity. The x-axis shows the degree of connectivity of the network and the y-axis shows the cumulative frequency of the appearance of a given degree. The degree of a node is the number of edges connected to that node. The cumulative degree distribution was indicative of a scale-free topology. The average path length of the network is 3.1.

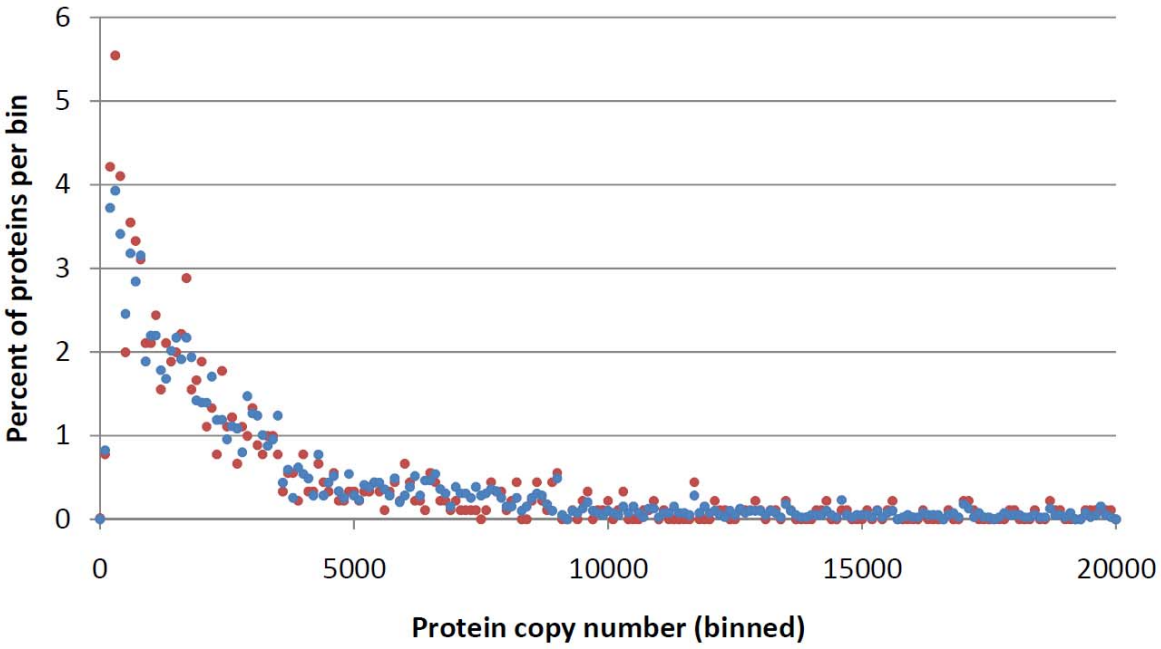

Fig. S3. Abundance distribution of responder phosphoproteins (proteins that contain "regulated" phosphopeptides). A comparison of the yeast proteome abundance distribution (blue) and the abundance of the regulated phosphoproteins as observed in this study (red, significance threshold FDR $\leq$ 0.015 and requiring at least a $\log_2$ 1.5-fold regulation or a full on or off response). The protein abundances were taken from Ghaemmaghami *et al.* (*26*). Proteins with more than 20,000 copies per cell are not displayed (the distribution of proteins with more than 20,000 copies per cell is similar between the analyzed phosphoprotein sets and the yeast proteome). The x-axis displays the protein copy number per cell, the y-axis the percentage of protein counts per copies per cell bin (with a bin size of 100) normalized by all of the proteins from the regulated phosphoprotein set or the data set of Ghaemmaghami *et al*. (*26*). The observations made for the responder phosphoproteins also held true if only the non-regulated phosphopeptides were analyzed, if the protein abundances were estimated by spectral counting as determined by Weiss *et al*. (*27*), or both.

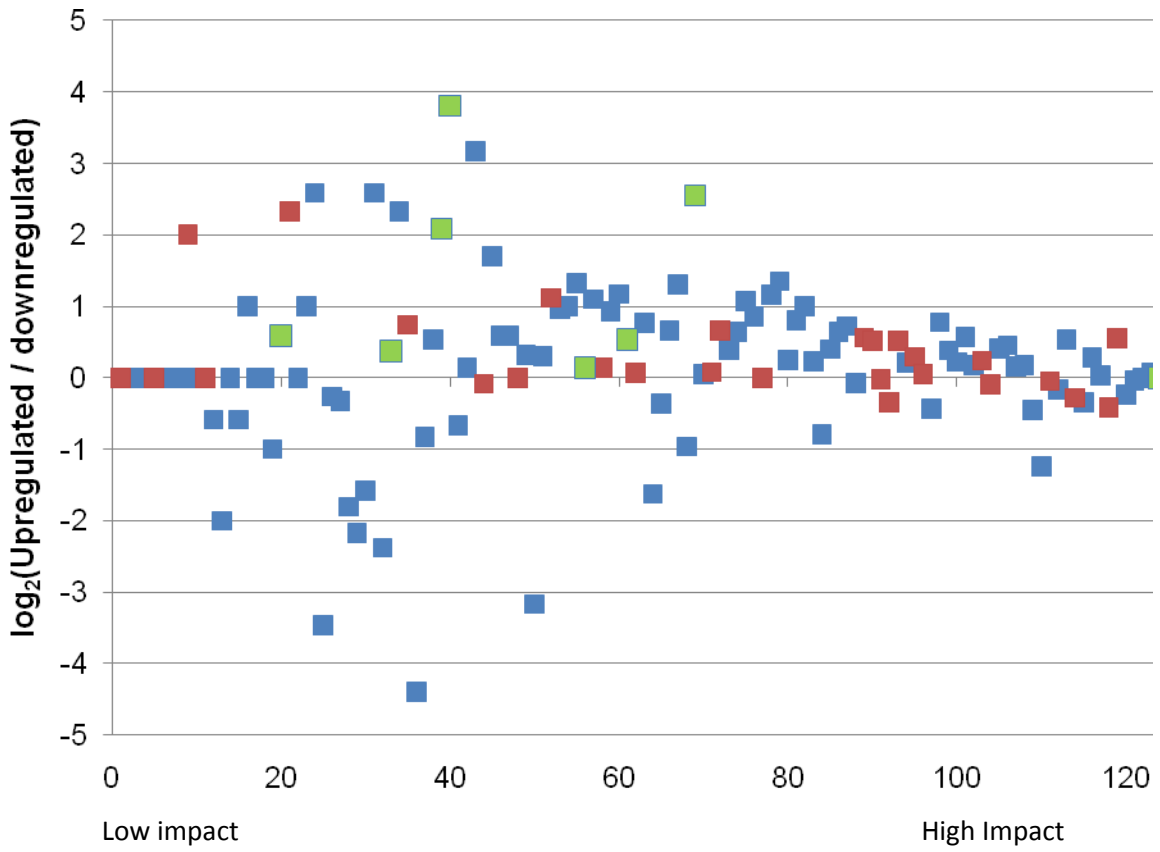

Fig. S4. Ratio of phosphopeptides that are reduced or increased in abundance. The y-axis shows the ratio [$\log_2$(number of increased phosphopeptides / number of decreased phosphopeptides)] and on the x-axis, the kinases and phosphatases are ordered according to the extent of their effect on the phosphoproteome (0 = lowest effect; 124 = highest effect, as calculated from the dataset in this study). The blue squares show the ratios for the kinases, the red squares show the ratios for the phosphatases, and the green squares show the ratios for the essential kinases. The higher ratios observed for the kinases and phosphatases with low activities were probably noise, because of the fewer regulated phosphopeptides observed. For this plot, relative regulation ("fold-changers") and complete disappearance ("on/off-responders", "vanishers") were not distinguished.

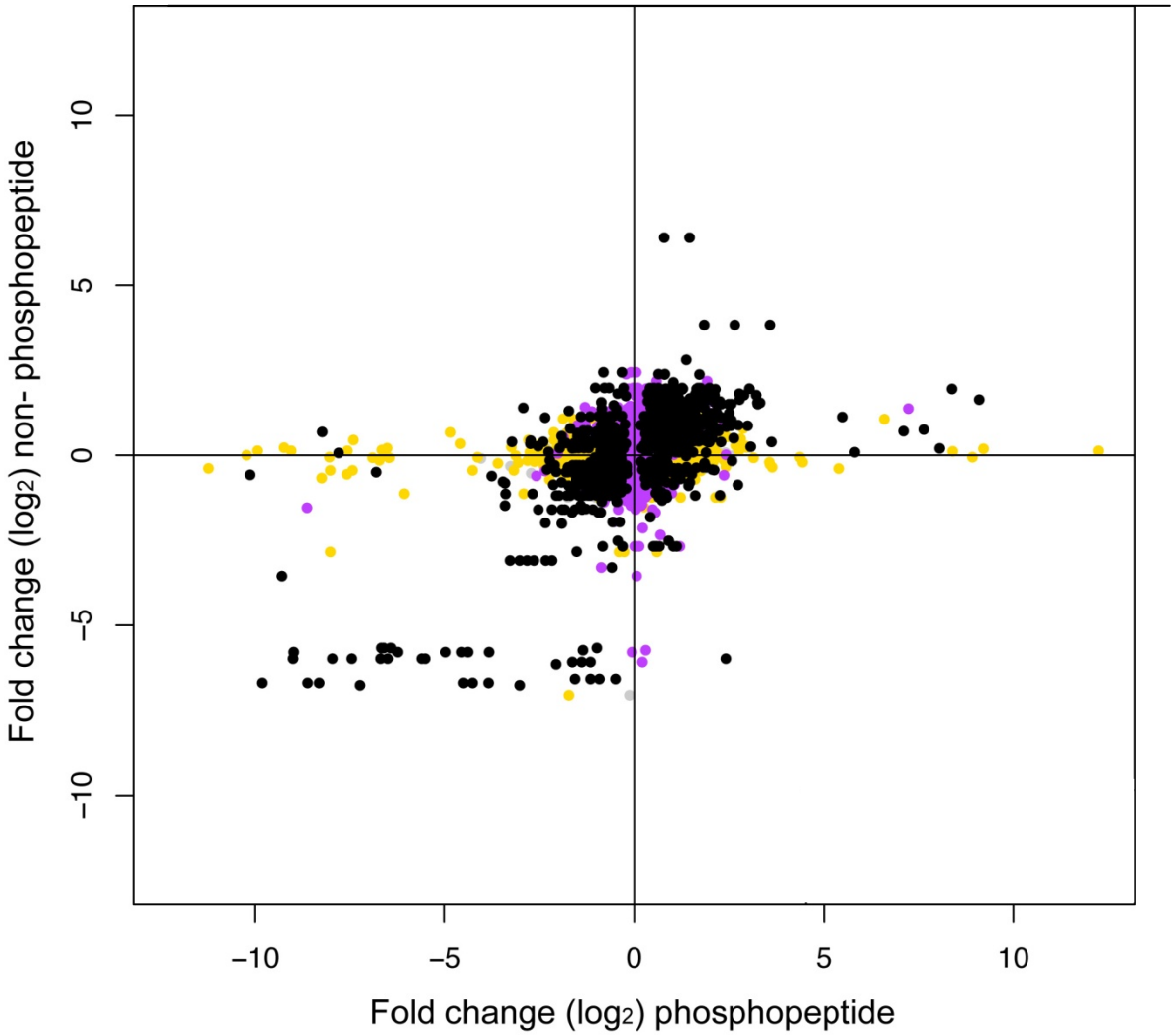

Fig. S5. Regulation of phosphopeptides versus regulation of protein abundance. Each dot corresponds to a measured phosphopeptide. The x-axis shows the fold-change (on a $\log_2$ scale) of the phosphopeptide and the y-axis shows the median change observed for all of the non-phosphorylated peptides that map to those particular proteins (both shown on a $\log_2$ scale). The color code illustrates whether the observed fold-change was significant in one or both of the measurements. ● denotes significant regulation detected in both phosphorylated and nonphosphorylated peptides; ● denotes significant regulation only for the phosphorylated peptide detected; ● denotes significant regulation only for the nonphosphorylated peptide detected; and ● denotes no significant regulation of any peptide detected.

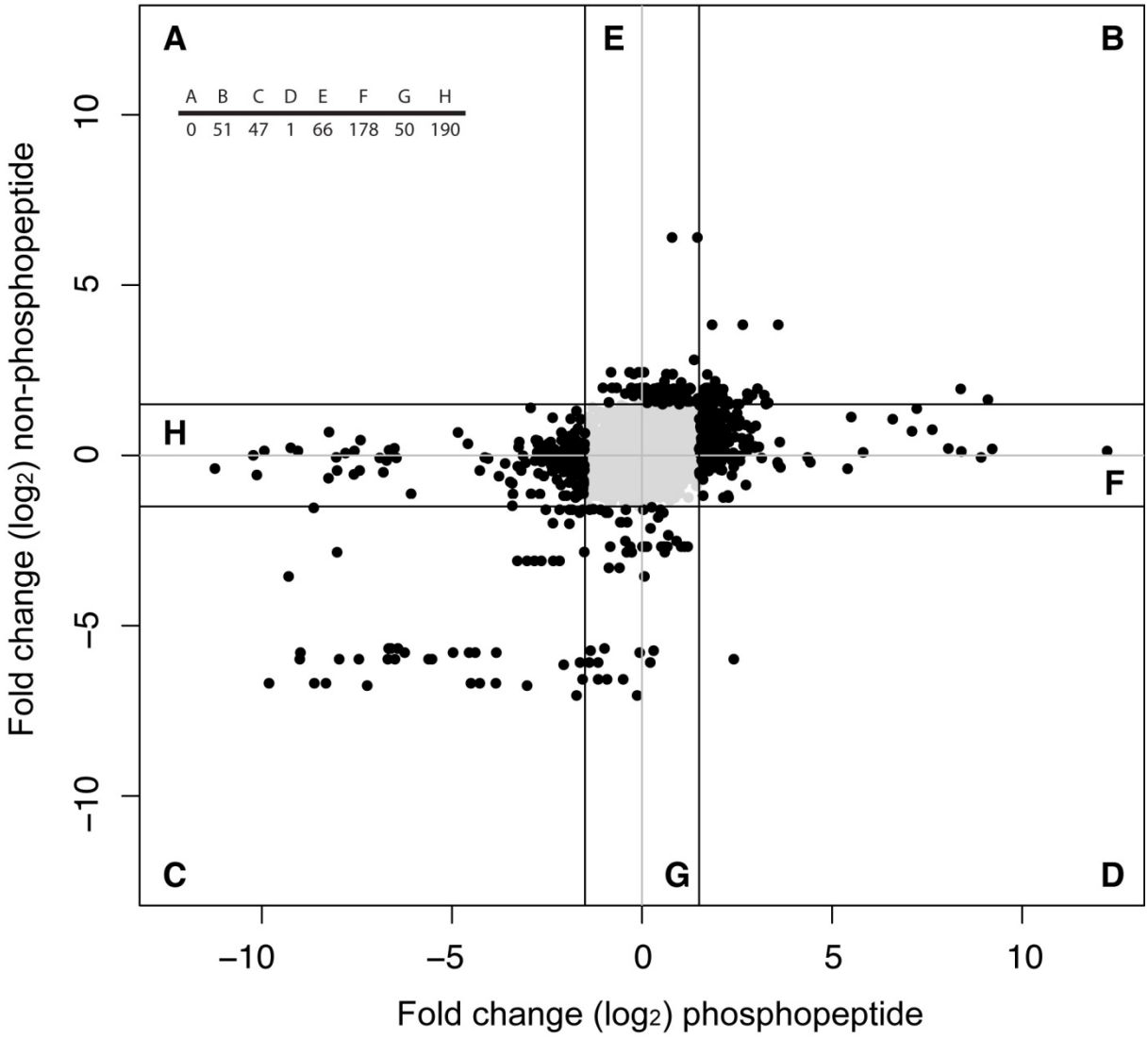

Fig. S6. Regulation of phosphopeptides versus regulation of protein abundance. The data shown are the same as those presented in fig. S5, but events that occurred below our standard fold-change cutoff are masked. This treatment enables us to see that the majority of the observed regulated changes in phosphopeptide abundance did not correspond to a change in protein abundance, but presumably in the occupancy of the phosphorylation sites. Note that this plot is based on a limited set of kinases (16 kinases), ranging from those that did not show any detectable impact on the phosphoproteome to those showing a large number of regulated phosphorylated peptides.

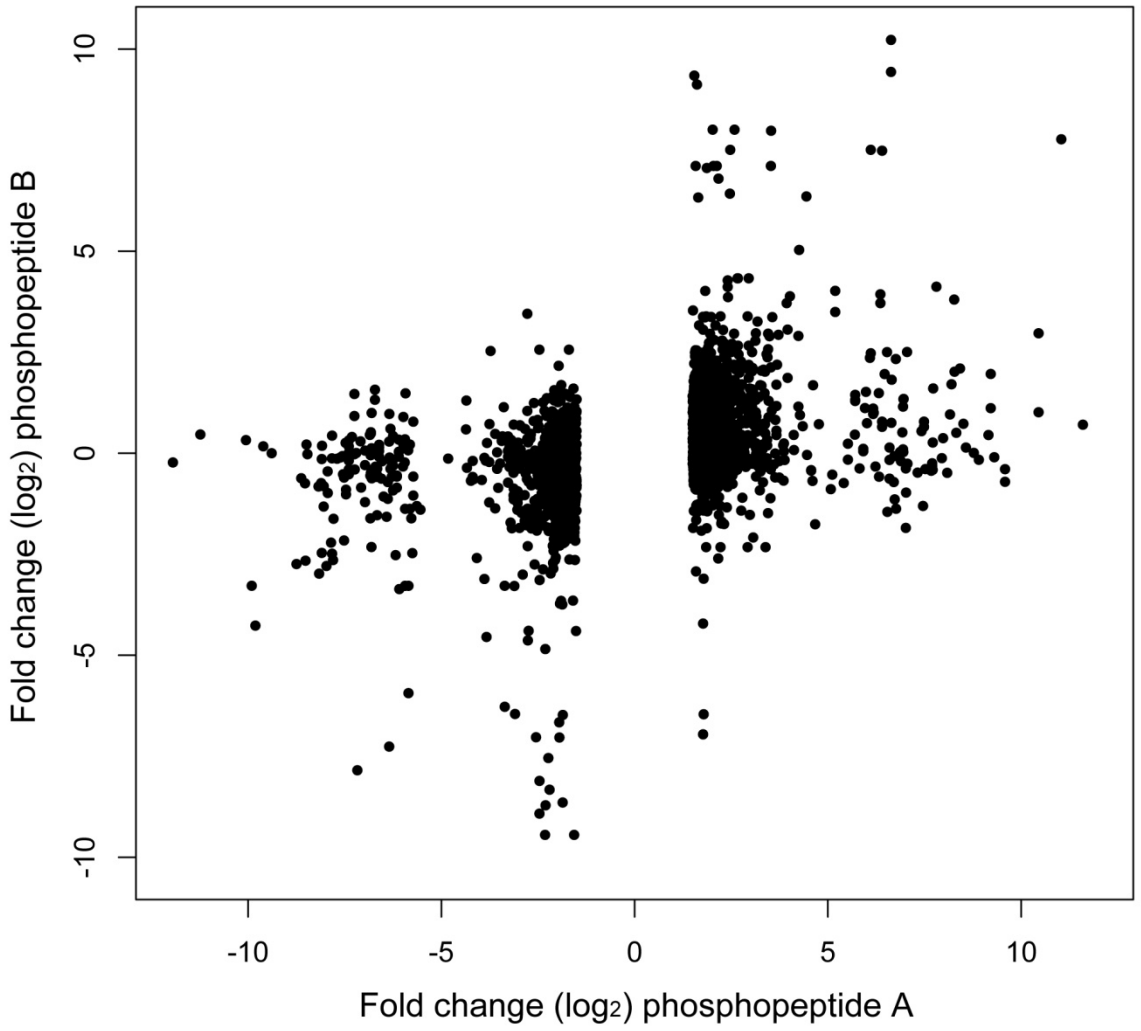

Fig. S7. Regulation of phosphopeptides that map to the same protein. On the x-axis are plotted phosphopeptides that were significantly regulated ($P < 0.015$; fold-change $\log_2 > 1.5$), whereas on the y-axis are plotted phosphopeptides that map to the corresponding phosphoprotein, irrespective of their significance or fold-change. In the majority of cases only one of the phosphopeptides that maps to a given phosphoprotein was regulated, indicating that the observed phosphorylation events were not due to a change in protein abundance.

Table S2. False discovery rate of peptide identification and specificity of phosphopeptide enrichment* for each analyzed phosphorylation pattern.

Kinase or phosphatase	Standard name	Group	FDR	% phosphopeptides*
YAL017W	PSK1	Other	0.05	86
YAR019C	CDC15	STE	0.03	79
YBL009W	ALK2		0.05	81
YBL016W	FUS3	CMGC	0.04	83
YBL056W	PTC3	STP	0.03	74
YBL088C	TEL1	Inositol Kinase	0.03	76
YBR028C		AGC	0.05	86
YBR059C	AKL1	Other	0.03	80
YBR097W	VPS15	Other	0.03	73
YBR125C	PTC4	STP	0.02	76
YBR160W	CDC28	CMGC	0.03	79
YBR274W	CHK1	Other	0.03	79
YBR276C	PPS1		0.04	83
YCR008W	SAT4	Other	0.04	82
YCR079W	PTC6	STP	0.04	85
YCR091W	KIN82	AGC	0.03	75
YDL006W	PTC1	STP	0.03	74
YDL025C	RTK1	Other	0.03	80
YDL028C	MPS1	Other	0.03	79
YDL047W	SIT4	STP	0.03	84
YDL079C	MRK1	CMGC	0.04	74
YDL101C	DUN1		0.03	74
YDL108W	KIN28	CMGC	0.03	78
YDL134C	PPH21	STP	0.05	77
YDL188C	PPH22	STP	0.05	85
YDL214C	PRR2	Other	0.04	85
YDL230W	PTP1	PTP	0.04	87
YDR075W	PPH3	STP	0.05	82
YDR122W	KIN1	CAMK	0.05	77
YDR247W	VHS1	Other	0.03	81
YDR283C	GCN2	Other	0.04	84
YDR466W	PKH3	AGC	0.03	83
YDR477W	SNF1	CAMK	0.03	87
YDR523C	SPS1	STE	0.03	81
YER129W	SAK1		0.04	82
YFR014C	CMK1	CAMK	0.05	86
YGL021W	ALK1		0.04	86
YGL059W	PKP2	Atypical PK	0.04	83

Table S2 continued.

Kinase or phosphatase	Standard name	Group	FDR	% phosphopeptides*
YGL179C	TOS3	CAMK	0.05	86
YGL180W	ATG1	Other	0.03	75
YGR040W	KSS1	CMGC	0.03	86
YGR123C	PPT1	STP	0.04	66
YGR188C	BUB1	Other	0.04	86
YGR203W	YCH1		0.04	82
YGR262C	BUD32	Microbial PK	0.03	76
YHR030C	SLT2	CMGC	0.06	82
YHR076W	PTC7		0.04	83
YHR082C	KSP1		0.05	78
YHR135C	YCK1	CKI	0.04	85
YIL035C	CKA1	Other	0.05	80
YIL042C	PKP1	Atypical PK	0.05	86
YIL095W	PRK1	Other	0.06	83
YIL113W	SDP1		0.04	75
YIR026C	YVH1		0.03	81
YJL095W	BCK1	STE	0.05	85
YJL106W	IME2	CMGC	0.02	75
YJL128C	PBS2	STE	0.02	71
YJL164C	TPK1	AGC	0.05	83
YJL165C	HAL5	Other	0.04	77
YJL187C	SWE1	Other	0.03	75
YJR059W	PTK2	Other	0.03	84
YJR066W	TOR1	Inositol Kinase	0.04	82
YKL048C	ELM1		0.03	73
YKL101W	HSL1	CAMK	0.04	82
YKL116C	PRR1	CAMK/EMK	0.05	83
YKL126W	YPK1	AGC	0.05	83
YKL139W	CTK1	CMGC	0.04	83
YKL161C	KDX1	CMGC	0.05	86
YKL166C	TPK3	AGC	0.04	84
YKL168C	KKQ8	Other	0.04	80
YKL171W	NNK1	Yeast PK	0.04	84
YKL198C	PTK1	Other	0.03	72
YLL010C	PSR1		0.05	77
YLL019C	KNS1	CMGC	0.05	86
YLR019W	PSR2		0.03	82
YLR096W	KIN2	CAMK	0.04	76

Table S2 continued.

Kinase or phosphatase	Standard name	Group	FDR	% phosphopeptides*
YLR113W	HOG1	CMGC	0.04	83
YLR240W	VPS34	Inositol Kinase	0.04	75
YLR248W	RCK2		0.03	74
YLR362W	STE11	STE	0.04	84
YLR433C	CNA1	STP	0.05	86
YML016C	PPZ1	STP	0.04	83
YML057W	CMP2	STP	0.05	86
YMR104C	YPK2	AGC	0.04	78
YMR139W	RIM11		0.03	82
YMR216C	SKY1	CMGC	0.04	83
YMR291W		CAMK	0.04	80
YNL020C	ARK1	Other	0.04	84
YNL032W	SIW14	PTP	0.03	86
YNL099C	OCA1		0.03	79
YNL154C	YCK2	CKI	0.04	65
YNL161W	CBK1	AGC	0.03	80
YNL298W	CLA4	STE	0.06	87
YNL307C	MCK1		0.04	73
YNR031C	SSK2	STE	0.04	78
YNR032W	PPG1	STP	0.05	86
YOL016C	CMK2	CAMK	0.04	84
YOL045W	PSK2	Other	0.03	86
YOL100W	PKH2	AGC	0.04	81
YOL113W	SKM1	STE	0.03	84
YOL128C	YGK3	CMGC	0.04	85
YOR061W	CKA2	Other	0.05	79
YOR090C	PTC5	STP	0.03	84
YOR119C	RIO1		0.03	80
YOR208W	PTP2	PTP	0.04	84
YOR231W	MKK1	STE	0.03	87
YOR233W	KIN4	CAMK	0.04	67
YOR267C	HRK1	Other	0.04	84
YOR351C	MEK1		0.03	84
YPL026C	SKS1		0.05	86
YPL031C	PHO85	CMGC	0.06	80
YPL042C	SSN3	CMGC	0.06	81
YPL140C	MKK2	STE	0.03	72
YPL141C	FRK1	CAMK	0.03	72
YPL150W		CAMK	0.04	85

Table S2 continued.

Kinase or phosphatase	Standard name	Group	FDR	% phosphopeptides*
YPL179W	PPQ1		0.05	82
YPL203W	TPK2	AGC	0.04	83
YPL204W	HRR25	CKI	0.03	78
YPL236C		Other	0.03	80
YPR054W	SMK1	CMGC	0.05	86
YPR073C	LTP1	DSP	0.03	79
YPR106W	ISR1	Yeast PK	0.05	82
YPR111W	DBF20	AGC	0.04	86
YPR161C	SGV1	CMGC	0.03	80

*"Specificity of phosphopeptide enrichment" / "% phosphopeptides": For a definition see Supplementary Materials description of "Database searches" and Bodenmiller *et al*. (*7*). The actual enrichment of phosphopeptides in the sample was likely even higher (for details see the Material and Methods).

Table S4. Significant coregulation of kinases and phosphatases.

Phosphatase	Standard name	Group	Kinase	Standard name	Group	*P* value	Spearman correlation coefficient
YDR075W	PPH3	STP	YIL095W	PRK1	Other	0.00E+00	0.97
YDL230W	PTP1	PTP	YIL042C	PKP1	Atypical PK	0.00E+00	0.95
YNL099C	OCA1		YGR262C	BUD32	Microbial PK	0.00E+00	0.95
YDL230W	PTP1	PTP	YPL026C	SKS1		0.00E+00	0.94
YML057W	CMP2	STP	YAL017W	PSK1	Other	0.00E+00	0.92
YCR079W	PTC6	STP	YGL059W	PKP2	Atypical PK	0.00E+00	0.9
YIR026C	YVH1		YDL025C	RTK1	Other	0.00E+00	0.89
YGR203W	YCH1		YGR262C	BUD32	Microbial PK	0.00E+00	0.86
YNL032W	SIW14	PTP	YDR477W	SNF1	CAMK	1.02E-04	0.85
YML057W	CMP2	STP	YIL042C	PKP1	Atypical PK	2.23E-04	0.87
YLL010C	PSR1		YIL035C	CKA1	Other	2.39E-04	0.88
YLL010C	PSR1		YOR061W	CKA2	Other	2.53E-04	0.71
YDL047W	SIT4	STP	YKL198C	PTK1	Other	4.84E-04	0.84
YML057W	CMP2	STP	YCR008W	SAT4	Other	5.77E-04	0.94
YLR019W	PSR2		YMR139W	RIM11		8.09E-04	0.82
YLL010C	PSR1		YOL045W	PSK2	Other	1.26E-03	0.72
YDR075W	PPH3	STP	YPL203W	TPK2	AGC	1.48E-03	0.75
YLL010C	PSR1		YKL166C	TPK3	AGC	2.04E-03	0.88
YNL099C	OCA1		YFR014C	CMK1	CAMK	4.25E-03	0.88
YDL230W	PTP1	PTP	YAL017W	PSK1	Other	9.45E-03	0.86
YNL099C	OCA1		YMR291W		CAMK	9.87E-03	0.76
YNL099C	OCA1		YIL042C	PKP1	Atypical PK	1.03E-02	0.84
YLR019W	PSR2		YKL171W	NNK1	Yeast PK	1.73E-02	0.98
YDL230W	PTP1	PTP	YDR477W	SNF1	CAMK	2.24E-02	0.76
YML057W	CMP2	STP	YOR231W	MKK1	STE	2.40E-02	0.74
YLR019W	PSR2		YIL042C	PKP1	Atypical PK	2.48E-02	0.88
YLR019W	PSR2		YOL045W	PSK2	Other	2.48E-02	0.88
YDL047W	SIT4	STP	YKL139W	CTK1	CMGC	3.47E-02	0.67
YDL230W	PTP1	PTP	YKL101W	HSL1	CAMK	3.83E-02	0.92
YLL010C	PSR1		YCR008W	SAT4	Other	4.12E-02	0.83
YGR203W	YCH1		YNL307C	MCK1		4.12E-02	0.81
YIR026C	YVH1		YKL166C	TPK3	AGC	4.12E-02	0.81
YNL099C	OCA1		YBR274W	CHK1	Other	4.12E-02	0.78
YLR019W	PSR2		YAL017W	PSK1	Other	4.12E-02	0.78
YDL047W	SIT4	STP	YGR262C	BUD32	Microbial PK	4.12E-02	0.75
YLR019W	PSR2		YFR014C	CMK1	CAMK	4.59E-02	0.85
YLL010C	PSR1		YOR231W	MKK1	STE	4.90E-02	0.73

Table S5. Overlap of data from this study with other data sets.

	All[#]	**Expected direction**		**Inverted direction**	
			Full response		**Full response**
STRING (*28*)	293 (285)**	162**	26**	131	14
SGD (*29*)	170 (168)	93*	22**	77	6
Fiedler (*30*)	39**	28**	4*	11	2
PhosphoGrid (*31*)	16*	10*	3	6	0

*Significant (P <0.05)
**Highly significant (P <0.01)
[#]Given numbers are observed regulatory events, whereas numbers in parentheses indicate the corresponding number of proteins.

Table S7. Overlap of possible direct targets with other data sets.

	All	**Expected direction**		**Inverted direction**	
			Full response		**Full response**
PhosphoGrid *(31)*	3	2	0	1	0
STRING *(28)*	109**	60**	14**	50*	3

*Significant (P <0.05)
**Highly significant (P <0.01)

Table S8. Effects of each kinase and phosphatase on the phosphoproteome. Growth speed is defined according to Hillenmeyer *et al*. (*24*) and phenotypes were defined according to Ohya *et al*. (*23*).

Systematic name	Standard name	Kinase or phosphatase group	Impact rank[1]	Growth phenotype*	Morphology phenotype*
YDL079C	MRK1	CMGC	1		
YML016C	PPZ1	STP	2		
YDR283C	GCN2	Other	4		
YJL187C	SWE1	Other	5		+
YBL056W	PTC3	STP	6		
YGL180W	ATG1	Other	7		
YKL116C	PRR1	CAMK/EMK	8		
YER129W	SAK1		9	+	
YPR073C	LTP1	DSP	10	+	+
YGR040W	KSS1	CMGC	11	+	
YHR076W	PTC7		12		
YDR122W	KIN1	CAMK	13		+
YOR267C	HRK1	Other	14		
YKL048C	ELM1		15		++
YLR248W	RCK2		16	+	
YOL016C	CMK2	CAMK	17		
YCR091W	KIN82	AGC	18	+	
YBR028C		AGC	19		+
YPL236C		Other	20		
YNL161W	CBK1	AGC	21		
YIL113W	SDP1		22		
YPL150W		CAMK	23		
YHR082C	KSP1		24		+
YOR351C	MEK1		25		
YDR247W	VHS1	Other	26	+	
YOL113W	SKM1	STE	27		+
YBL009W	ALK2		28		
YLR362W	STE11	STE	29		
YDL028C	MPS1	Other	30		
YDR523C	SPS1	STE	31		++
YDL101C	DUN1		32		
YPL141C	FRK1	CAMK	33		
YPR161C	SGV1	CMGC	34		

[1]Highest impact = 124, lowest impact = 1. *Compared to wild-type; "+", strong; "++", very strong (see Material and Methods).

Table S8 continued.

Systematic name	Standard name	Kinase or phosphatase group	Impact rank	Growth phenotype*	Morphology phenotype*
YGL179C	TOS3	CAMK	35		
YOR090C	PTC5	STP	36		+
YOL128C	YGK3	CMGC	37		
YKL161C	KDX1	CMGC	38		+
YKL168C	KKQ8	Other	39		+
YPL204W	HRR25	CKI	40		
YOR119C	RIO1		41		
YBL088C	TEL1	Inositol Kinase	42		+
YLR113W	HOG1	CMGC	43	+	+
YJL128C	PBS2	STE	44		+
YGR123C	PPT1	STP	45		
YBL016W	FUS3	CMGC	46		++
YJL095W	BCK1	STE	47	++	+
YPR106W	ISR1	Yeast PK	48	+	
YPL179W	PPQ1		49		
YHR030C	SLT2	CMGC	50	++	+
YDL214C	PRR2	Other	51		
YJL106W	IME2	CMGC	52		
YDL006W	PTC1	STP	53		++
YMR104C	YPK2	AGC	54		+
YGL021W	ALK1		55		
YPR054W	SMK1	CMGC	56	+	
YAR019C	CDC15	STE	57		
YOR233W	KIN4	CAMK	58		
YOR208W	PTP2	PTP	59	+	
YBR059C	AKL1	Other	60	+	
YNL020C	ARK1	Other	61		+
YBR160W	CDC28	CMGC	62		
YNR032W	PPG1	STP	63		+
YJR059W	PTK2	Other	64	+	
YLR096W	KIN2	CAMK	65		
YJL164C	TPK1	AGC	66		+
YGR188C	BUB1	Other	67		
YBR097W	VPS15	Other	68		++

[1] Highest impact = 124, lowest impact = 1. *Compared to wild type; “+”, strong; “++”, very strong (see Material and Methods).

Table S8 continued.

Systematic name	Standard name	Kinase or phosphatase group	Impact rank	Growth phenotype*	Morphology phenotype*
YPR111W	DBF20	AGC	69		
YDL108W	KIN28	CMGC	70		
YMR139W	RIM11		71		
YNL032W	SIW14	PTP	72	+	+
YBR125C	PTC4	STP	73		
YJL165C	HAL5	Other	74	++	
YDL025C	RTK1	Other	75		
YNR031C	SSK2	STE	76		+
YLL019C	KNS1	CMGC	77		
YLR019W	PSR2		78		
YBR274W	CHK1	Other	79		
YMR216C	SKY1	CMGC	80	++	++
YPL140C	MKK2	STE	81		
YFR014C	CMK1	CAMK	82		
YJR066W	TOR1	Inositol Kinase	83		
YIL095W	PRK1	Other	84		
YOL100W	PKH2	AGC	85		
YNL298W	CLA4	STE	86		++
YDR466W	PKH3	AGC	87		+
YMR291W		CAMK	88		
YGL059W	PKP2	Atypical PK	89		
YDR075W	PPH3	STP	90	++	
YLR433C	CNA1	STP	91		
YBR276C	PPS1		92		+
YML057W	CMP2	STP	93		
YDL188C	PPH22	STP	94		
YCR008W	SAT4	Other	95	+	
YNL099C	OCA1		96	++	
YCR079W	PTC6	STP	97	+	
YLR240W	VPS34	Inositol Kinase	98		+
YIL035C	CKA1	Other	99	+	+
YPL031C	PHO85	CMGC	100		+
YPL026C	SKS1		101		+
YOR061W	CKA2	Other	102	+	++

[1] Highest impact = 124, lowest impact = 1. * compared to wild type; "+" strong, "++" very strong (See Material and Methods).

Table S8 continued.

Systematic name	Standard name	Kinase or phosphatase group	Impact rank	Growth phenotype*	Morphology phenotype*
YOR231W	MKK1	STE	103		++
YDL134C	PPH21	STP	104		
YGR203W	YCH1		105		
YKL101W	HSL1	CAMK	106		++
YAL017W	PSK1	Other	107		
YKL171W	NNK1	Yeast PK	108		+
YKL166C	TPK3	AGC	109		
YHR135C	YCK1	CKI	110	+	
YIL042C	PKP1	Atypical PK	111		+
YDL230W	PTP1	PTP	112		
YPL203W	TPK2	AGC	113		
YNL307C	MCK1		114	++	+
YIR026C	YVH1		115	+	++
YGR262C	BUD32	Microbial PK	116		++
YKL126W	YPK1	AGC	117	++	++
YPL042C	SSN3	CMGC	118		++
YDL047W	SIT4	STP	119		++
YLL010C	PSR1		120		+
YDR477W	SNF1	CAMK	121	++	
YKL198C	PTK1	Other	122		
YOL045W	PSK2	Other	123	+	
YKL139W	CTK1	CMGC	124		++

[1]Highest impact = 124; lowest impact = 1.

*Compared to wild-type; “+”, strong; “++”, very strong (see Material and Methods).

Table S9. Enrichment of biological process among the low-impact kinases (bottom half). n.d., not determined.

Biological process	***P* value**	**Corresponding *P* value for bottom half kinases**
protein kinase cascade	1.9E-11	5.8E-05
MAPKKK cascade	3.9E-10	8.6E-04
osmosensory signaling pathway	5.6E-10	1.8E-01
cell surface receptor linked signal transduction	1.8E-09	9.8E-02
primary metabolic process	3.4E-09	3.0E-07
cellular metabolic process	1.1E-08	8.3E-06
MAPKKK cascade during osmolarity sensing	2.4E-08	9.6E-02
metabolic process	5.9E-08	3.4E-05
regulation of MAP kinase activity	9.3E-08	n.d.
response to osmotic stress	1.2E-07	5.8E-01
regulation of cell cycle	2.4E-07	1.2E-04
regulation of molecular function	2.6E-07	1.3E-02
regulation of protein kinase activity	4.9E-07	2.7E-01
intracellular signaling cascade	5.6E-07	5.6E-07
regulation of kinase activity	5.9E-07	2.8E-01
regulation of conjugation	7.1E-07	2.8E-01
regulation of conjugation with cellular fusion	7.1E-07	2.8E-01
regulation of multi-organism process	7.1E-07	2.8E-01
regulation of transferase activity	8.4E-07	2.9E-01
regulation of catalytic activity	1.5E-06	5.1E-02
response to stimulus	1.9E-06	4.7E-07
regulation of cell division	2.1E-06	3.3E-01
response to pheromone	4.2E-06	7.1E-02
cell cycle	5.5E-06	5.5E-06
regulation of cellular component organization and biogenesis	6.4E-06	5.0E-03
inactivation of MAPK activity during osmolarity sensing	7.2E-06	n.d.
inactivation of MAPK activity	7.2E-06	n.d.
protein amino acid autophosphorylation	7.2E-06	4.5E-02
negative regulation of MAP kinase activity	7.2E-06	n.d.
negative regulation of protein kinase activity	1.4E-05	n.d.
negative regulation of transcription by pheromones	1.4E-05	n.d.
negative regulation of transcription from RNA polymerase II promoter by pheromones	1.4E-05	n.d.

Biological process	***P* value**	**Corresponding *P* value for bottom half kinases**
cell cycle checkpoint	1.7E-05	2.2E-04
response to stress	1.8E-05	1.8E-05
negative regulation of kinase activity	2.5E-05	n.d.
regulation of cell morphogenesis	3.3E-05	1.6E-03
regulation of anatomical structure morphogenesis	3.3E-05	1.6E-03
negative regulation of transferase activity	3.9E-05	n.d.
regulation of developmental process	4.9E-05	2.1E-03
cell division	5.5E-05	8.8E-03
negative regulation of specific transcription from RNA polymerase II promoter	5.9E-05	n.d.
negative regulation of gene-specific transcription	5.9E-05	n.d.
regulation of meiosis	6.9E-05	n.d.
regulation of meiotic cell cycle	8.1E-05	n.d.
negative regulation of conjugation	8.2E-05	n.d.
negative regulation of conjugation with cellular fusion	8.2E-05	n.d.
negative regulation of multi-organism process	8.2E-05	n.d.
regulation of transcription by pheromones	8.3E-05	n.d.
regulation of transcription from RNA polymerase II promoter by pheromones	8.3E-05	n.d.

Table S10. Enrichment of biological process among the high-impact kinases (top half). n.d., not determined.

Biological process	***P* value**	**Corresponding *P* value for top half kinases**
interphase of mitotic cell cycle	3.3E-09	2.7E-01
G1/S transition of mitotic cell cycle	4.9E-09	3.4E-01
interphase	5.2E-09	2.9E-01
primary metabolic process	3.0E-07	3.4E-09
response to stimulus	4.7E-07	1.9E-06
intracellular signaling cascade	5.6E-07	5.6E-07
peptidyl-serine phosphorylation	7.3E-07	n.d.
peptidyl-serine modification	7.3E-07	n.d.
cell cycle phase	1.2E-06	1.8E-02
mitotic cell cycle	1.4E-06	8.7E-02
cell cycle process	4.1E-06	3.0E-02
cell cycle	5.5E-06	5.5E-06
cellular metabolic process	8.3E-06	1.1E-08
cellular ion homeostasis	1.1E-05	3.0E-01
cellular chemical homeostasis	1.1E-05	3.0E-01
ion homeostasis	1.6E-05	3.2E-01
chemical homeostasis	1.7E-05	3.2E-01
response to stress	1.8E-05	1.8E-05
regulation of biological quality	2.1E-05	4.8E-03
cellular developmental process	2.1E-05	3.9E-04
cell morphogenesis	2.2E-05	1.2E-04
anatomical structure morphogenesis	2.2E-05	1.2E-04
cellular structure morphogenesis	2.2E-05	1.2E-04
anatomical structure development	2.2E-05	1.2E-04
metabolic process	3.4E-05	5.9E-08
protein kinase cascade	5.8E-05	1.9E-11
regulation of mitotic cell cycle	6.0E-05	1.5E-01

Table S12. Overview of the entire data set.

	Total number	Regulated	Not regulated
Phosphoproteins	1,677 [1]	1,029 [2]	648 [3]
Phosphopeptides	11,374 [4]	3,824 [5]	7,550 [6]
Phospho-Events	158,168 [7]	8,814 [8]	149,354 [9]

[1]Number of all identified phosphoproteins in the dataset. [2]Number of all phosphoproteins that had at least one regulated phosphorylation site. [3]Number of all phosphoproteins that did not have any regulated phosphorylation site. [4]Number of all identified phosphopeptides in the dataset. [5]Number of all phosphopeptides that were considered to be regulated. [6]Number of all phosphopeptides that were not regulated. [7]Number of all individually identified phosphorylation sites per kinase or phosphatase. [8]Number of all individually identified regulated phosphorylation sites per kinase or phosphatase. [9]Number of all individually identified phosphorylation sites that were not regulated per kinase or phosphatase.

References

1. A. H. Tong, C. Boone, Synthetic genetic array analysis in Saccharomyces cerevisiae. *Methods Mol. Biol.* **313**, 171-192 (2006).
2. A. C. Bishop, J. A. Ubersax, D. T. Petsch, D. P. Matheos, N. S. Gray, J. Blethrow, E. Shimizu, J. Z. Tsien, P. G. Schultz, M. D. Rose, J. L. Wood, D. O. Morgan, K. M. Shokat, A chemical switch for inhibitor-sensitive alleles of any protein kinase. *Nature* **407**, 395-401 (2000).
3. M. E. Burkard, C. L. Randall, S. Larochelle, C. Zhang, K. M. Shokat, R. P. Fisher, P. V. Jallepalli, Chemical genetics reveals the requirement for Polo-like kinase 1 activity in positioning RhoA and triggering cytokinesis in human cells. *Proc. Natl. Acad. Sci. USA* **104**, 4383-4388 (2007).
4. K. R. Benjamin, C. Zhang, K. M. Shokat, I. Herskowitz, Control of landmark events in meiosis by the CDK Cdc28 and the meiosis-specific kinase Ime2. *Genes Dev.* **17**, 1524-1539 (2003).
5. T. Tamguney, C. Zhang, D. Fiedler, K. Shokat, D. Stokoe, Analysis of 3-phosphoinositide-dependent kinase-1 signaling and function in ES cells. *Exp. Cell. Res.* **314**, 2299-2312 (2008).
6. Y. Liu, C. Kung, J. Fishburn, A. Z. Ansari, K. M. Shokat, S. Hahn, Two cyclin-dependent kinases promote RNA polymerase II transcription and formation of the scaffold complex. *Mol. Cell Biol.* **24**, 1721-1735 (2004).
7. B. Bodenmiller, L. N. Mueller, M. Mueller, B. Domon, R. Aebersold, Reproducible isolation of distinct, overlapping segments of the phosphoproteome. *Nat. Methods* **4**, 231-237 (2007).
8. A. Keller, A. I. Nesvizhskii, E. Kolker, R. Aebersold, Empirical statistical model to estimate the accuracy of peptide identifications made by MS/MS and database search. *Anal. Chem.* **74**, 5383-5392 (2002).
9. J. E. Elias, S. P. Gygi, Target-decoy search strategy for increased confidence in large-scale protein identifications by mass spectrometry. *Nat. Methods* **4**, 207-214 (2007).
10. S. A. Beausoleil, J. Villen, S. A. Gerber, J. Rush, S. P. Gygi, A probability-based approach for high-throughput protein phosphorylation analysis and site localization. *Nat. Biotechnol.* **24**, 1285-1292 (2006).
11. P. J. Ulintz, B. Bodenmiller, P. C. Andrews, R. Aebersold, A. I. Nesvizhskii, Investigating MS2/MS3 matching statistics: a model for coupling consecutive stage mass spectrometry data for increased peptide identification confidence. *Mol. Cell. Proteomics* **7**, 71-87 (2008).
12. B. Bodenmiller, D. Campbell, B. Gerrits, H. Lam, M. Jovanovic, P. Picotti, R. Schlapbach, R. Aebersold, PhosphoPep--a database of protein phosphorylation sites in model organisms. *Nat. Biotechnol.* **26**, 1339-1340 (2008).
13. B. Bodenmiller, J. Malmstrom, B. Gerrits, D. Campbell, H. Lam, A. Schmidt, O. Rinner, L. N. Mueller, P. T. Shannon, P. G. Pedrioli, C. Panse, H. K. Lee, R. Schlapbach, R. Aebersold, PhosphoPep--a phosphoproteome resource for systems biology research in Drosophila Kc167 cells. *Mol. Syst. Biol.* **3**, 139 (2007).
14. L. N. Mueller, O. Rinner, A. Schmidt, S. Letarte, B. Bodenmiller, M. Y. Brusniak, O. Vitek, R. Aebersold, M. Muller, SuperHirn - a novel tool for high resolution LC-MS-based peptide/protein profiling. *Proteomics* **7**, 3470-3480 (2007).
15. M. Y. Brusniak, B. Bodenmiller, D. Campbell, K. Cooke, J. Eddes, A. Garbutt, H. Lau, S. Letarte, L. N. Mueller, V. Sharma, O. Vitek, N. Zhang, R. Aebersold, J. D. Watts, Corra: Computational framework and tools for LC-MS discovery and targeted mass spectrometry-based proteomics. *BMC Bioinformatics* **9**, 542 (2008).
16. G. Smyth, Linear Models and Empirical Bayes Methods for Assessing Differential Expression in Microarray Experiments. *Stat. Appl. Gen.Mol. Biol.* **3**, Article 3 (2004).
17. M. Y. Brusniak, B. Bodenmiller, D. Campbell, K. Cooke, J. Eddes, A. Garbutt, H. Lau, S. Letarte, L. N. Mueller, V. Sharma, O. Vitek, N. Zhang, R. Aebersold, J. D. Watts, Corra: Computational framework and tools for LC-MS discovery and targeted mass spectrometry-based proteomics. *BMC Bioinformatics* **9**, 542 (2008).
18. G. K. Smyth, J. Michaud, H. S. Scott, Use of within-array replicate spots for assessing differential expression in microarray experiments. *Bioinformatics* **21**, 2067-2075 (2005).
19. Y. Benjamini, Y. Hochberg, Controlling The False Discovery Rate - Practical And Powerful Approach To Multiple Testing. *J. R. Stat. Soc. Ser. B-Methodol.* **57**, 289-300 (1995).

20. Y. Benjamini, D. Yekutieli, The control of the false discovery rate in multiple testing under dependency. *Annal. Stat.* (2001).
21. L. Shi, L. H. Reid, W. D. Jones, R. Shippy, J. A. Warrington, S. C. Baker, P. J. Collins, F. de Longueville, E. S. Kawasaki, K. Y. Lee, Y. Luo, Y. A. Sun, J. C. Willey, R. A. Setterquist, G. M. Fischer, W. Tong, Y. P. Dragan, D. J. Dix, F. W. Frueh, F. M. Goodsaid, D. Herman, R. V. Jensen, C. D. Johnson, E. K. Lobenhofer, R. K. Puri, U. Schrf, J. Thierry-Mieg, C. Wang, M. Wilson, P. K. Wolber, L. Zhang, S. Amur, W. Bao, C. C. Barbacioru, A. B. Lucas, V. Bertholet, C. Boysen, B. Bromley, D. Brown, A. Brunner, R. Canales, X. M. Cao, T. A. Cebula, J. J. Chen, J. Cheng, T. M. Chu, E. Chudin, J. Corson, J. C. Corton, L. J. Croner, C. Davies, T. S. Davison, G. Delenstarr, X. Deng, D. Dorris, A. C. Eklund, X. H. Fan, H. Fang, S. Fulmer-Smentek, J. C. Fuscoe, K. Gallagher, W. Ge, L. Guo, X. Guo, J. Hager, P. K. Haje, J. Han, T. Han, H. C. Harbottle, S. C. Harris, E. Hatchwell, C. A. Hauser, S. Hester, H. Hong, P. Hurban, S. A. Jackson, H. Ji, C. R. Knight, W. P. Kuo, J. E. LeClerc, S. Levy, Q. Z. Li, C. Liu, Y. Liu, M. J. Lombardi, Y. Ma, S. R. Magnuson, B. Maqsodi, T. McDaniel, N. Mei, O. Myklebost, B. Ning, N. Novoradovskaya, M. S. Orr, T. W. Osborn, A. Papallo, T. A. Patterson, R. G. Perkins, E. H. Peters, R. Peterson, K. L. Philips, P. S. Pine, L. Pusztai, F. Qian, H. Ren, M. Rosen, B. A. Rosenzweig, R. R. Samaha, M. Schena, G. P. Schroth, S. Shchegrova, D. D. Smith, F. Staedtler, Z. Su, H. Sun, Z. Szallasi, Z. Tezak, D. Thierry-Mieg, K. L. Thompson, I. Tikhonova, Y. Turpaz, B. Vallanat, C. Van, S. J. Walker, S. J. Wang, Y. Wang, R. Wolfinger, A. Wong, J. Wu, C. Xiao, Q. Xie, J. Xu, W. Yang, S. Zhong, Y. Zong, W. Slikker, Jr., The MicroArray Quality Control (MAQC) project shows inter- and intraplatform reproducibility of gene expression measurements. *Nat. Biotechnol.* **24**, 1151-1161 (2006).
22. A. Gordon, A. Colman-Lerner, T. E. Chin, K. R. Benjamin, R. C. Yu, R. Brent, Single-cell quantification of molecules and rates using open-source microscope-based cytometry. *Nat. Methods* **4**, 175-181 (2007).
23. Y. Ohya, J. Sese, M. Yukawa, F. Sano, Y. Nakatani, T. L. Saito, A. Saka, T. Fukuda, S. Ishihara, S. Oka, G. Suzuki, M. Watanabe, A. Hirata, M. Ohtani, H. Sawai, N. Fraysse, J. P. Latge, J. M. Francois, M. Aebi, S. Tanaka, S. Muramatsu, H. Araki, K. Sonoike, S. Nogami, S. Morishita, High-dimensional and large-scale phenotyping of yeast mutants. *Proc. Natl. Acad. Sci. USA* **102**, 19015-19020 (2005).
24. M. E. Hillenmeyer, E. Fung, J. Wildenhain, S. E. Pierce, S. Hoon, W. Lee, M. Proctor, R. P. St Onge, M. Tyers, D. Koller, R. B. Altman, R. W. Davis, C. Nislow, G. Giaever, The chemical genomic portrait of yeast: uncovering a phenotype for all genes. *Science* **320**, 362-365 (2008).
25. A. L. Oberg, O. Vitek, Statistical design of quantitative mass spectrometry-based proteomic experiments. *J. Proteome Res.* **8**, 2144-2156 (2009).
26. S. Ghaemmaghami, W. K. Huh, K. Bower, R. W. Howson, A. Belle, N. Dephoure, E. K. O'Shea, J. S. Weissman, Global analysis of protein expression in yeast. *Nature* **425**, 737-741 (2003).
27. M. Weiss, S. Schrimpf, M. O. Hengartner, M. J. Lercher, C. von Mering, Shotgun proteomics data from multiple organisms reveals remarkable quantitative conservation of the eukaryotic core proteome. *Proteomics* **10**, 1297-1306.
28. L. J. Jensen, M. Kuhn, M. Stark, S. Chaffron, C. Creevey, J. Muller, T. Doerks, P. Julien, A. Roth, M. Simonovic, P. Bork, C. von Mering, STRING 8--a global view on proteins and their functional interactions in 630 organisms. *Nucleic Acids Res.* **37**, D412-416 (2009).
29. J. M. Cherry, C. Ball, S. Weng, G. Juvik, R. Schmidt, C. Adler, B. Dunn, S. Dwight, L. Riles, R. K. Mortimer, D. Botstein, Genetic and physical maps of Saccharomyces cerevisiae. *Nature* **387**, 67-73 (1997).
30. D. Fiedler, H. Braberg, M. Mehta, G. Chechik, G. Cagney, P. Mukherjee, A. C. Silva, M. Shales, S. R. Collins, S. van Wageningen, P. Kemmeren, F. C. Holstege, J. S. Weissman, M. C. Keogh, D. Koller, K. M. Shokat, N. J. Krogan, Functional organization of the S. cerevisiae phosphorylation network. *Cell* **136**, 952-963 (2009).
31. C. Stark, T. C. Su, A. Breitkreutz, P. Lourenco, M. Dahabieh, B. J. Breitkreutz, M. Tyers, I. Sadowski, PhosphoGRID: a database of experimentally verified *in vivo* protein

phosphorylation sites from the budding yeast *Saccharomyces cerevisiae*. *Database* **58**, (2010).